NeuroImage 202 (2019) 116028

Contents lists available at ScienceDirect

NeuroImage

journal homepage: www.elsevier.com/locate/neuroimage

Motion sickness-susceptible participants exposed to coherent rotating dot patterns show excessive N2 amplitudes and impaired theta-band phase synchronization

Yue Wei [a,c], Yuka O. Okazaki [d], Richard H.Y. So [a,b,c,*], Winnie C.W. Chu [e], Keiichi Kitajo [d,f,g]

[a] HKUST-Shenzhen Research Institute, 9 Yuexing First Road, South Area, Hi-tech Park, Nanshan, Shenzhen, 518057, China
[b] Department of Industrial Engineering and Decision Analytics, The Hong Kong University of Science and Technology, Hong Kong, China
[c] Bio-Engineering Graduate Program, School of Engineering, The Hong Kong University of Science and Technology, Hong Kong, China
[d] RIKEN CBS-TOYOTA Collaboration Center, RIKEN Center for Brain Science, Wako, Saitama, 351-0198, Japan
[e] Department of Imaging and Interventional Radiology, Prince of Wales Hospital, Hong Kong, China
[f] Division of Neural Dynamics, Department of System Neuroscience, National Institute for Physiological Sciences, National Institutes of Natural Sciences, Okazaki, Aichi, 444-8585, Japan
[g] Department of Physiological Sciences, School of Life Science, The Graduate University for Advanced Studies (SOKENDAI), Okazaki, 444-8585, Japan

ARTICLE INFO

Keywords:
Visually induced motion sickness
Vection
Electroencephalography
N2
Theta-band phase synchronization

ABSTRACT

Visually induced motion sickness (VIMS) can occur via prolonged exposure to visual stimulation that generates the illusion of self-motion (vection). Not everyone is susceptible to VIMS and the neural mechanism underlying susceptibility is unclear. This study explored the differences of electroencephalographic (EEG) signatures between VIMS-susceptible and VIMS-resistant groups. Thirty-two-channel EEG data were recorded from 12 VIMS-susceptible and 15 VIMS-resistant university students while they were watching two patterns of moving dots: (1) a coherent rotation pattern (vection-inducing and potentially VIMS-provoking pattern), and (2) a random movement pattern (non-VIMS-provoking control). The VIMS-susceptible group exhibited a significantly larger increase in the parietal N2 response when exposed to the coherent rotating pattern than when exposed to control patterns. In members of the VIMS-resistant group, before vection onset, global connectivity from all other EEG electrodes to the right-temporal-parietal and to the right-central areas increased, whereas after vection onset the global connectivity to the right-frontal area reduced. Such changes were not observed in the susceptible group. Further, the increases in N2 amplitude and the identified phase synchronization index were significantly correlated with individual motion sickness susceptibility. Results suggest that VIMS susceptibility is associated with systematic impairment of dynamic cortical coordination as captured by the phase synchronization of cortical activities. Analyses of dynamic EEG signatures could be a means to unlock the neural mechanism of VIMS.

1. Introduction

Continuous exposure to visual motion stimulation spanning a wide field-of-view (FOV) can provoke symptoms similar to motion sickness among stationary viewers. This has been referred to as visually induced motion sickness (VIMS) (Hettinger et al., 1990; Keshavarz et al., 2015b; So and Ujike, 2010; Zhang et al., 2015). VIMS is frequently reported among users of virtual reality systems, with typical symptoms including disorientation, oculomotor disturbance and gastrointestinal discomfort (Chen et al., 2011; Griffin, 1990; Kennedy et al., 1993; Stanney et al., 2002). Susceptibility to VIMS varies among individuals and is stimuli dependent (Chen et al., 2015; Diels and Howarth, 2011; Graeber and Stanney, 2002; Guo et al., 2017; Ji et al., 2009; Kennedy et al., 2010; Keshavarz et al., 2014, 2015b; Yokota et al., 2005). As the popularity of virtual reality increases and concerns about VIMS grow (Rebenitsch and Owen, 2016; So and Ujike, 2010), it is important to understand the neural mechanism underlying VIMS. In particular, the ISO working group on image safety called for more fundamental research on the etiology of VIMS (ISO, 2005).

The mechanisms underlying VIMS susceptibility are not fully understood. Humans perceive self-motion through the integration of information from multiple modalities (e.g. visual, vestibular, somatosensory and proprioceptive). The most widely accepted 'sensory conflict theory'

* Corresponding author. HKUST-Shenzhen Research Institute, 9 Yuexing First Road, South Area, Hi-tech Park, Nanshan, Shenzhen, 518057, China.
E-mail address: rhyso@ust.hk (R.H.Y. So).

https://doi.org/10.1016/j.neuroimage.2019.116028
Received 2 November 2018; Received in revised form 10 July 2019; Accepted 16 July 2019
Available online 18 July 2019

Abbreviations (in alphabetic order except rc and vc):

BC	Baseline condition
CC	Control condition
RC	Rotation condition
VC	Vection condition
CRS	Coherent rotating dot pattern stimulation
EEG	Electroencephalographic
FOV	Field of view
MSSQ	Motion Sickness Susceptibility Questionnaire
MT+	Middle temporal (MT) complex
NOI	Node of interest
PLV	Phase-locking value
PM	Parietal midline
TP	Temporal-parietal
SSQ	Simulator Sickness Questionnaire
VEP	Visual evoked potential
VIMS	Visually induced motion sickness

predicts that between-modality and within-modality conflicts would lead to motion sickness if these accumulated conflicts exceed a threshold (Carriot et al., 2013; DeAngelis and Angelaki, 2012; Oman and Cullen, 2014). In the case of VIMS, visual motion spanning a wide FOV is presented to stationary viewers, thus visual input is in conflict with other senses (Brandt et al., 1998; Dichgans and Brandt, 1978; Hettinger et al., 1990). These conflicts, if accumulated, can cause VIMS among susceptible individuals, while individuals who are resistant to VIMS are hypothesized to be able to reduce sensory conflicts to below the sickness threshold through coordination between visual and non-visual modalities (Brandt et al., 2002, 1998). However, the dynamic neural basis underlying VIMS susceptibility and the development of sensory conflicts in this hypothesis have not yet been thoroughly examined.

Most former studies have focused on locating the brain areas associated with VIMS. These studies have identified local blood-oxygen-level-dependent (BOLD) or electroencephalographic (EEG) signals oscillating components that are correlated with VIMS ratings (Chen et al., 2009; Chuang et al., 2016; Napadow et al., 2013; Sheehan et al., 2009) or located cortical areas showing differential responses between VIMS-susceptible and VIMS-resistant groups (Farmer et al., 2015). However, little has been reported on the functional connectivity mapping among relevant cortical regions for groups with different levels of VIMS susceptibility, and how this functional connectivity mapping changes across cortical regions and over time under potentially VIMS-provoking stimulation. Miyazaki et al. (2015), the only exception, restricted their exploration to inter-hemispheric synchronization within visually-sensitive cortices (Miyazaki et al., 2015). The functional connectivity mapping among cortical regions responsible for different modalities (e.g., visual and vestibular) has not been thoroughly studied. As VIMS involves coordination between different sensory inputs and their integration (central integration) (Brandt et al., 1998), it is important to examine cortical synchronization among widely distributed brain regions (e.g. visual, vestibular and somatosensory) and investigate how these synchronization patterns develop across cortical regions and over time under coherent visual motion stimulation spanning a large FOV (capable of triggering VIMS given prolonged exposure). As the phase synchronization of EEG rhythms can reflect cortical coordination and sensory integration (Murray and Wallace, 2011; Varela et al., 2001), this study utilized EEG phase synchrony to capture the dynamic neural mechanisms underlying VIMS susceptibility.

In order to isolate the cortical coordination associated with VIMS susceptibility, we need to measure and control for two important confounding factors. The first one is the illusion of self-motion (known as vection). VIMS-provoking visual stimulation often induce vection with various individualized latencies (Chen et al., 2011; Keshavarz et al., 2015b). Although VIMS and vection have been frequently reported together (Chen et al., 2011; Nooij et al., 2017; Palmisano et al., 2018; Wei et al., 2018), the nature of their relationship is not fully understood. VIMS can occur with or without vection, and conversely, vection can occur with and without VIMS (Keshavarz et al., 2015b). According to the sensory integration perspective, the onset of vection might indicate a different stage of sensory integration from the initial period when stationary individuals exposed to visual stimuli still feel that they are not moving (Brandt et al., 1998). At the moment when they start to perceive self-motion, their inner perception models are reportedly being updated toward the visual input (Kleinschmidt et al., 2002; Thilo et al., 2003). Brain activities before and/or after the onset of vection have been the subject of many studies (Berti et al., 2018; Keshavarz et al., 2015a; Kleinschmidt et al., 2002; Stróżak et al., 2016; Thilo et al., 2003). While these studies have set different objectives, one common finding is that the occurrence of vection is associated with changes in neural activities. Hence, it is necessary to record and analyze the data before and after the onset of vection for each individual to isolate the confounding effects caused by variations in vection perception. Second, participants in former neural imaging studies reported severe nausea symptoms after exposing to VIMS-provoking stimuli (Farmer et al., 2015; Miyazaki et al., 2015; Napadow et al., 2013). Since visually-induced nausea is linked to massive increases in the cortical hemodynamic response (Le et al., 2017; Wilkins, 2016), it can introduce confounding effects on the reported cortical BOLD responses (Farmer et al., 2015; Napadow et al., 2013) and inter-hemispheric desynchronization (Miyazaki et al., 2015). Consequently, it is necessary to control for both the onset of vection and nausea.

In this study, we tested whether the strength and range of cortical coordination between visual and other cortical regions are significantly affected among VIMS-susceptible participants, while controlling for the onset of vection and nausea. In particular, we recorded EEG signals when VIMS-susceptible or VIMS-resistant participants were exposed to short periods (up to 1 min) of coherent rotating dot pattern stimulation (CRS) until vection onset (see Fig. 1). The participants were allowed sufficient rest between exposures to avoid nausea. Continuous exposures to this type of CRS for 20 min have been shown to induce symptoms of VIMS. Hence, this type of CRS is also referred to as vection-inducing and potentially VIMS-provoking stimulation. As theta-band synchronization is related to sensory conflict (Aitake et al., 2011a; Araújo et al., 2002; Jo et al., 2017; White et al., 2012) and motion sickness (Chelen et al., 1993), theta band phase synchronization analyses were also conducted in this study. Based on the literature, we hypothesize a stronger phase synchronization between electrodes placed over visual areas and other cortical areas during exposure to CRS than during exposure to the control visual stimuli (hypothesis H1a). Moreover, as enhanced cortical coordination dynamics could reflect the process underlying sensory integration and conflicts reduction, we further hypothesize that VIMS-resistant participants would show stronger supporting evidence for hypothesis H1a than VIMS-susceptible participants (H1b). As theta-band synchronization is closely related to the detection of sensory mismatch (Aitake et al., 2011b; Liang et al., 2017), we hypothesize that the dynamic change in theta band phase synchronization before and after vection onset is organized differently between the VIMS-resistant group and the VIMS-susceptible group (hypothesis H2).

2. Method

2.1. Participants

A total of 27 right-handed university students with 20/20 (or corrected) eyesight were recruited with complete informed consent. Twelve participants who scored above the 70th percentile in the short-form version of the Motion Sickness Susceptibility Questionnaire (MSSQ) formed the VIMS-susceptible group, while another 15 participants who

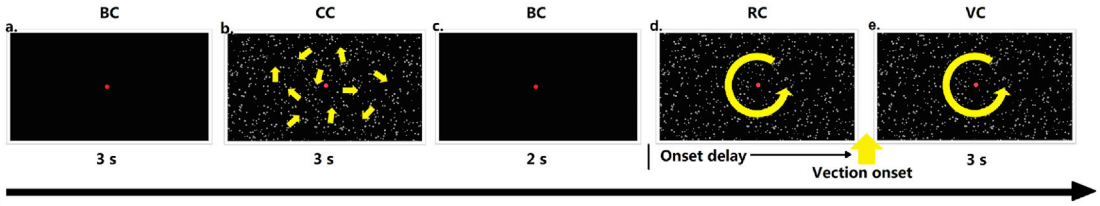

Fig. 1. Stimuli and trial procedure. (Note that the arrows are added here to illustrate the movement of dots and were not presented on the screen during the experiment) (a) BC: baseline condition; (b) CC: control condition; (c) BC: baseline condition; (d) RC: rotating condition; (e) VC: vection condition.

scored below the 30th percentile in MSSQ made up the VIMS-resistant group. None of the participants had vestibular injury or were under medical treatment. None of them considered themselves to be heavy video game players (spending more than 3 h per week on computer games) or to have rich experience with large-screen visual motion stimuli. All of them attained 20/20 visual acuity (Vision Tester: Stereo Optical CO. Inc. U.S.A., Model, 2000). Both groups had a mix of gender (VIMS-susceptible: 54.5% male; VIMS-resistant: 60% male). There were no significant intergroup differences in gender and age (Table 1).

2.2. Motion Sickness Susceptibility Questionnaire (MSSQ)

Farmer et al. (2015) noted that participants with higher MSSQ scores reported significantly higher self-rated levels of VIMS. The significant positive correlations between MSSQ scores and VIMS levels are consistent with many studies (Hwang et al., 2017; Nesbitt et al., 2017) as well as our pilot study (Zhao, 2017). In this study, participants were screened by their VIMS susceptibility based on the score in the short-form version of the MSSQ (MSSQ-Short) (Golding, 1998). In MSSQ-Short, participants completed both the child scale (MSSQ_C) based on their experience before the age of 12, and the adult scale (MSSQ_A) based on their experience over the last 10 years only. The total score (MSSQ_T) equals to the sum of scores in MSSQ_C and MSSQ_A (Golding, 1998).

Table 1
Demographics, VIMS reports and vection perception of the VIMS-susceptible and VIMS-resistant groups.

	VIMS susceptible	VIMS resistant	*P*
Age (years)	24.5 ± 1.2	24.3 ± 2.7	0.893
Gender (% male)	54.5%	60%	0.791
MSSQ score			
Child (0–27)	17.4 ± 3.7	1.7 ± 1.3	<0.001
Adult (0–27)	12.3 ± 5.7	1.3 ± 1.2	<0.001
Total (0–54)	29.6 ± 8.0	3.0 ± 2.1	<0.001
Pre-SSQ total score (0–120)	0.5 ± 0.7	2.6 ± 3.8	0.073
Post-SSQ total score (0–120)	2.4 ± 2.6	4.6 ± 5.2	0.221
Pre-Post paired t-test p value	0.022	0.210	
Vection report			
Intensity (1–5)	2.9 ± 0.6	2.8 ± 0.6	0.666
% of trials with strong vection (trials with intensity>3)	32.5 ± 39.0	37.2 ± 39.2	0.766
Onset delay (seconds)	9.7 ± 9.2	8.6 ± 4.3	0.716
Std. dev. of individual onset delay (seconds)	4.1 ± 4.3	4.3 ± 4.4	0.926
Response rate (%)	99.6 ± 1.3	99.3 ± 1.9	0.560
Average blocks completed*	11.33	11.73	0.782
Total clean epochs	282.9 ± 48.0	309.4 ± 51.5	0.195
EEG quality (% clean epochs)	72.7%	76.8%	0.320

Except the MSSQ score, none of the group comparisons are significant with two-tailed independent-sample *t*-tests (* the two-sided Wilcoxon signed-rank tests when the data are not normally distributed); note that the SSQ score increased only for the susceptible group after the experiment (two-tailed paired-sample *t*-test, $p = 0.022$), but the severity of sickness remained very low (2.4 in 120), and was not significantly different from that for the VIMS-resistant group.

2.3. Visual stimuli

Grey dots (diameter: 0.5–1.3° of FOV) were displayed in random positions on a black background. For CRS, all of the grey dots rotated anticlockwise at an angular velocity of 32°/s around the center of the screen. We chose roll rotation because human seldom experience this type of motion without vestibular and other non-visual stimulation. Based on sensory conflict theory (Reason, 1978), motion profiles that are novel to the individual are more likely to provoke motion sickness. This rotating condition (RC) with the CRS has been examined previously (Du, 2016), where the same experimental setup and a similar random dot pattern were able to induce VIMS after prolonged continuous exposure (Fig. 1d). Our CRS can provoke VIMS and vection given prolonged exposure as verified in a pilot study. Moreover, the pilot study examined whether MSSQ scores can predict the level of VIMS provoked by our visual stimulation. We exposed 18 participants with known MSSQ scores (recruited from the same pool of university students as that in the main study) to visual stimuli similar to those used in main study. All participants reported vection. Participants who scored higher than median scores of MSSQ_T in the population, all reported significant increases in nausea after 20-min of exposure. Significant correlations were also reported between MSSQ scores and rated nausea ($r = 0.57$) (Zhao, 2017). For the control condition (CC), similar randomly-positioned dots were used but instead of all rotating in the same direction, they moved in random directions at the same tangential velocities as their counterparts in the RC (Fig. 1b) (Brandt et al., 1998; Zhao, 2017).

2.4. Apparatus, tasks and procedures

All stimuli were presented on a 46-inch LCD monitor (screen size: 102.1 × 57.5 cm; FOV: 93.5° × 61.8°; viewing distance: 48 cm) with 700–750 dots visible under both conditions. Participants were instructed to fixate a red dot at the center (diameter: 0.6° of FOV, Fig. 1d). A chin-rest was used to limit head and body movement. To eliminate visual distractions, we turned off all the lights and covered the TV and the participants with a large black curtain. All stimuli and EEG synchronization triggers were programmed in MATLAB using the Psychtoolbox-3 extensions (Brainard, 1997; Pelli, 1997). The experiment took place inside an acoustic booth (a 1400-A-CT chamber custom-built by the Industrial Acoustics Company Limited). The metal wireframe of the booth provided electromagnetic shielding to the EEG electrodes against background noise. The booth had an inner and an outer compartment and all computers were placed in the outer compartment to reduce electrical interference. The LCD display was shielded with grounded wire mesh.

As illustrated in Fig. 1, each trial started with the baseline black background condition (BC) for 3 (Fig. 1a), followed by the control condition (CC) for 3 s (Fig. 1b), the BC again for 2 s (Fig. 1c) and finally the rotating condition (RC, Fig. 1d). Participants were educated about the illusion of vection and were instructed to press a button with their right-index fingers to indicate the onset of roll vection. After the onset response was received, the RC stimulus would continue for another 3 s before terminating. This was referred to as the vection condition (VC, Fig. 1e). If a participant did not report vection (i.e., no button was pressed), the stimulus would terminate at 1 min. This happened in less than 1% of the

trials. The whole experiment was divided into separated blocks. Each block consisted of 12 trials with sufficient rest in between to minimize any nausea. Twenty-four participants completed all 12 blocks. Three participants did not finish all 12 blocks for non-health-related reasons and some of the data for one participant were lost due to a software crash. Two of them were in the susceptible group, while the other two were in the resistant group (see Table 1 for a summary). We did not exclude these participants because there were still enough data for each of them for analysis. All procedures were approved by the ethics committee of the Hong Kong University of Science and Technology and performed in accordance with the Declaration of Helsinki.

2.5. Response measures

2.5.1. EEG signal recordings and preprocessing

During stimuli presentation, the EEG signals were recorded together with the horizontal and vertical electrooculograms using a NuAmps amplifier (DC-coupled, 22 bits, monopolar) connected to 32-channel Ag/AgCl sintered electrodes (Quik-Cap, Compumedics Neuroscan) placed according to the international 10-10 system referenced to linked mastoid electrodes. Impedances between all other channels and the ground channel (AFz) were kept below 5 kΩ. Raw data were digitized at a sampling rate of 1000 Hz and a bandwidth of DC-260 Hz, and then filtered offline using a finite impulse response filter with passband from 1.6 Hz to 47 Hz. Data were segmented into epochs starting from 1.5 s prior to the onset (0s) of each condition (CC/RC/VC) and ending at 3s with the BC corrected for the 1.5 s before onset. Independent components analysis was applied to these epochs using EEGLAB (Delorme and Makeig, 2004), and components identified as artifacts (blinking, eye movements and generic discontinuities) were removed using the automatic toolbox ADJUST (Mognon et al., 2011). The epochs contaminated by other artifacts were rejected using the moving-window peak-to-peak method (window size: 200 ms; step: 50 ms; threshold: ±100 μV) and the extreme value of remaining components (threshold: ±20 μV). One participant (a female in the susceptible group) was excluded due to extensive motion artifacts (>50% epochs rejected). The average number of epochs remaining for each condition and their standard deviations were as follows: CC (91.6 ± 22.2), RC (105.5 ± 19.0) and VC (101.0 ± 21.1). Current source density analyses (the order of spline m = 4; precision = 1.0e-5) were then performed at each electrode position to reduce the influence of volume conduction (Kayser and Tenke, 2006a, 2006b).

2.5.2. Visual evoked potential (VEP) analysis

To analyze the visual evoked potential (VEP), the remaining clean epochs were trimmed to smaller windows (−0.5~1s) and averaged for the two types of visual stimulation (CC and RC). Several components with distinct time-space properties were identified based on the grand averaged topography of VEP results (see Fig. 2a and b). The P1, N1/N2 and P3 components at the parietal electrodes were analyzed, and the center electrodes were selected for each component in later analyses. Specifically, the mean amplitudes of P1 (time window: 135–195 ms), the early N2 (time window: 195–250 ms) and P3 (time window: 250–395 ms) at electrode Pz, the bilateral late N2 (time window: 260–335 ms) at electrode P7/P8, and the late P3 (time window: 330–410 ms) at electrode P3/P4 were calculated for each individual.

2.5.3. Phase synchronization and network analysis

Wavelet analyses were conducted to obtain the instantaneous phase for each time point in clean epochs applying Morlet's mother function. We applied a constant ratio $f/\sigma_f = 6$ with f ranging from 2 to 46 Hz (in steps of 1 Hz), where $\sigma_f = 1/2\pi\sigma_t$ and σ_t is the standard deviation of the Gaussian window (Kawasaki et al., 2014;Lachaux, Jean-Philippe Rodriguez et al., 2000). In order to assess functional connectivity mediating information integration between distant cortical areas, the phase synchronization was evaluated between each pair of electrodes at each time point in the epoch (−1~3s) of all conditions (RC, CC, and VC) using phase-locking values (PLVs) (Lachaux et al., 1999; Totah et al., 2013). Specifically, for time point t, frequency f, and electrodes j and k, across the N available epochs, we calculated the PLV from the following equation:

$$PLV_{j,k}(f,t) = N^{-1}\left|\sum_{1}^{N} e^{i\left[\varphi_j(t)-\varphi_k(t)\right]}\right|$$

where $\varphi(t)$ is phase at t, i is $\sqrt{-1}$, and $|\ |$ is the complex modulus. As we focused on the theta band, the PLVs are averaged for theta-band frequencies (4–7 Hz) and transformed into PLV_z according to Rayleigh's Z value (Fisher, 1993; Totah et al., 2013) to correct for the bias associated with the number of epochs:

$$PLV_z = N \times PLV^2 \ (N: number\ of\ epochs)$$

2.5.3.1. Node strength in the dynamic phase synchronization network. After obtaining the PLV_z, we constructed the dynamical phase synchronization networks, where the 30 EEG electrodes were set as nodes and the edge between each node pair at every time point was weighted by the PLV_z. The dynamic strength of each node was calculated by summing the weights of all connections to that node at each time point. In order to spatiotemporally verify that CRS induces greater node strength in the phase synchrony network than CC stimulation, we conducted cluster-based permutation tests on node strength between CC and RC for each VIMS group using the Fieldtrip toolbox (Oostenveld et al., 2011). The cluster-based permutation test has been shown to be a better analytical tool for EEG data with minimal multi-comparison problem and the flexibility to incorporate biophysically constraints (Maris and Oostenveld, 2007). We conducted the cluster-based permutation tests to determine whether the observed difference in cluster-size between conditions was large enough to reject the null hypothesis as following procedures (Genovese et al., 2002). The tests followed three main steps. First, the cluster-size for observed data were obtained by the following sub-steps: (i) every element (30 nodes: 30-EEG channels; 4500 time points: −1500–3000 ms) in node strength matrices between CC and RC conditions was compared using two-tailed paired t-test for the VIMS-resistant group and the VIMS-susceptible group respectively; (ii) the contiguous negative and positive clusters in the matrices (with a threshold of uncorrected p-value < 0.05) were identified; and (iii) the cluster-sizes were calculated by summing up all the t-values within the cluster. Second, to obtain the null-distribution of the test statistic on cluster-size, repeated (i) to (iii) 2000 times using random matrices generated by permuting two condition labels (CC and RC here) within each participant. Finally, with the 97.5th percentile of the null distribution as the level of statistical significance, we identified the significant clusters of observed data. Similar cluster-based permutation tests were applied to determine if node strength was difference before and after vection onset across spatial electrodes in the VIMS-resistant group and the VIMS-susceptible group.

2.5.3.2. Node degree in binary subnetworks connected to nodes of interest (NOI). In addition to the dynamic strength of phase synchronization (node strength), we further investigated the distribution properties of phase synchronization by analysing the subnetwork containing the links connected only to the nodes of interest (NOIs) with significantly high node strength across all time points (see Fig. 3a). Centers of significant nodes in the cluster analyses conveniently provided such NOIs (e.g., RC/CC, Fig. 3b–f; before/after vection onset, Fig. 5b). To better observe the range and distribution of strong dynamic links in subnetworks, we transformed them into binary network by applying threshold masks. The threshold masks were obtained by conducting permutation tests (Sun et al., 2012; Winkler et al., 2016) for each edge (node pair). Specifically, we shuffled the condition labels (RC/CC; Before/After vection onset) of

the edge weights (average PLV_z of each window) for each participant 2000 times and obtained the group mean difference between conditions to approximate the permutation distribution under the null hypothesis (no difference between conditions). We calculated grand averaged threshold masks which only allowed edges whose weight differences (RC − CC; Before vection onset − After vection onset) were above 97.5% or below 2.5% in the permutation distributions to be kept in the positive or negative subnetwork of each NOIs respectively (see Appendix I for positive and negative grand average subnetworks in each window and each group). By applying these threshold masks to each participant, we obtained positive and negative binary subnetworks and calculated their node degrees (number of connections) for each participant, where a larger node degree reflects a wider range of phase-locking connections.

2.5.4. Reports of vection and VIMS

During the visual stimulation, subjects had to press a button to indicate the onset of vection. The response rate was calculated as the percentage of trials with a response (i.e., indicated a vection onset). The average response rates exceeded 99% for both the VIMS-resistant group and the VIMS-susceptible group (see Table 1).

Participants were trained to report vection intensity after each trial completed, based on a vection magnitude scale adapted from former studies (Webb and Griffin, 2003) (1 = no vection; 5 = saturated vection; see Appendix II for details). The onset latency of vection was calculated as the time between the start of the RC and when the button was pressed for each trial. VIMS symptoms were monitored with a pre-exposure Simulator Sickness Questionnaire (SSQ) before the start of the experiment and a post-exposure SSQ (Kennedy et al., 1993) after all (trials) were completed. The total scores of pre-and post-SSQ were calculated for each participant.

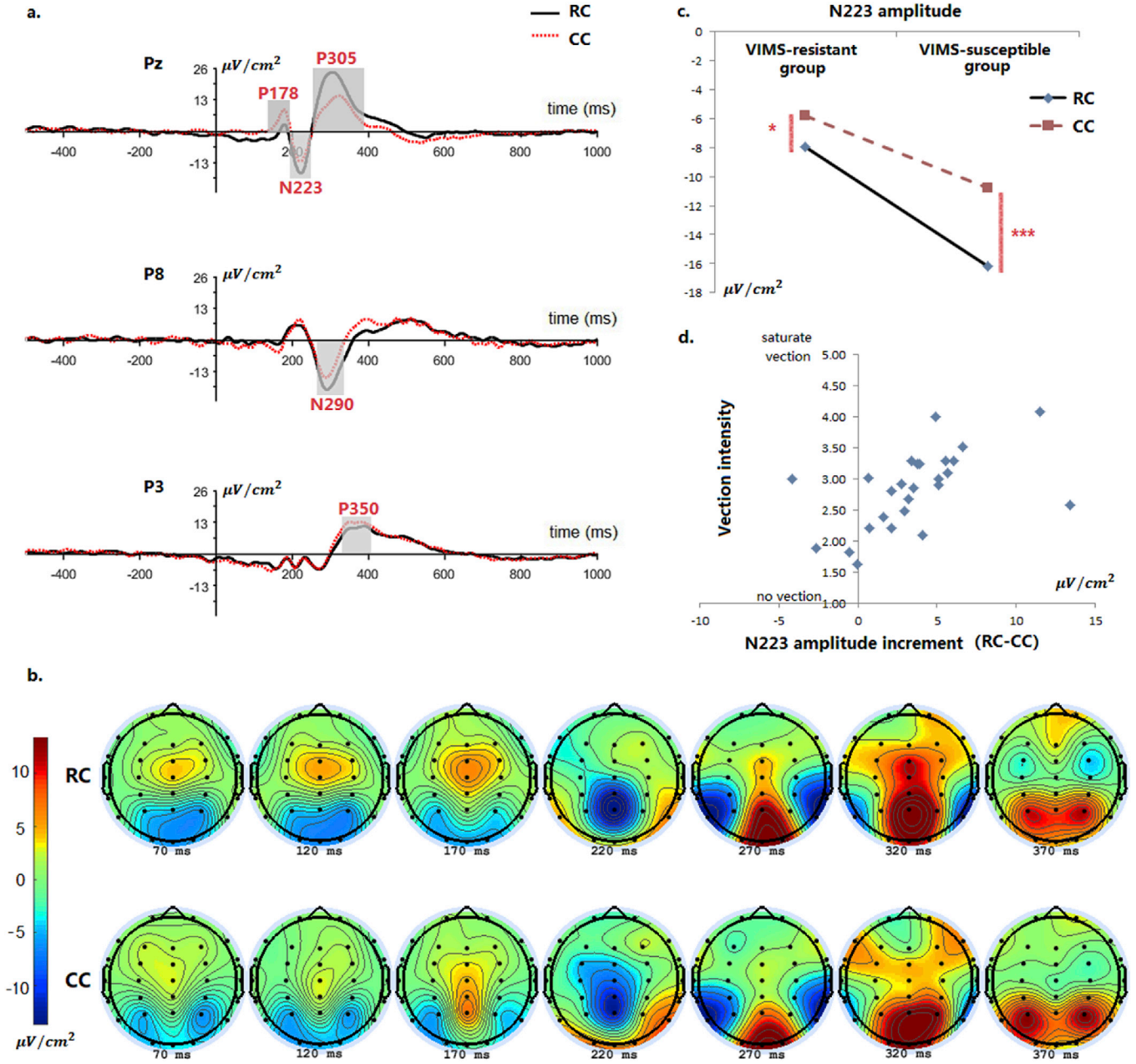

Fig. 2. VEP results for N = 26 participants. (a) Average VEP for two stimulus conditions (RC and CC) at electrodes of interest (shaded areas illustrate the time window for each component). (b) Topography of VEP amplitude map under the RC and CC. (c) Effect of interaction of VIMS group × visual condition on N223 amplitude (***p = 0.001; *p < 0.05). (d) Scatter plot of vection intensity and the increase in N223 (amplitude in the RC minus amplitude in the CC). Onset of vection is defined as 0s.

3. Results

3.1. Behavioral results and subjective reports

The mean and standard deviation of vection intensity, vection onset delay, percentage of trials with strong vection (trials with intensity > 3), MSSQ scores and pre-/post-SSQ scores of each VIMS-susceptible and resistant groups are reported in Table 1, along with the *p*-values of between-group (VIMS-susceptible vs VIMS-resistant) two-tailed independent-sample *t*-tests (or Wilcoxon signed-rank tests cases in cases where the data are not normally distributed). Only the MSSQ scores of all scales are significantly higher for the VIMS-susceptible group ($p < 0.001$). The demographic variables, vection reports and VIMS symptoms evaluated using the post-exposure SSQ were not significantly different between the two groups.

3.2. VEP data

Two-way mixed-measures ANOVA including the factors of visual condition (RC/CC) and VIMS group (VIMS-resistant/VIMS-susceptible) was conducted for each of the middle components at the Pz electrode (Fig. 2a & b). For P1 in the 135–195 ms window (P178, Fig. 2a), the RC showed a significantly suppressed amplitude compared with the CC [$F(1,24) = 22.41,\ p < 0.001$]. No interaction or VIMS group effects were found for P178. For N2 in the 195–250 ms window (N223), the amplitude in the RC was significantly increased compared with that in the CC [$F(1,24) = 31.21,\ p < 0.001$], while the main effect for VIMS group was not significant, possibly due to large individual variations. Moreover, the interaction of visual condition × VIMS group was significant, where the VIMS-susceptible group showed a larger N223 increase than the resistant group [$F(1,24) = 5.92,\ p = 0.023$, see Fig. 2c]. The simple main effect for visual condition was significant for both the resistant group ($p = 0.011$) and the susceptible group ($p = 0.001$), while none of the simple main effects for VIMS group were significant. For P3 in the 250–395 ms windows (P305, Fig. 2a), the amplitude in the RC was significantly larger than that in the CC [$F(1,24) = 31.48,\ p < 0.001$], with no group and interaction effects.

Three-way mixed-measures ANOVA including the factors of visual condition (RC/CC), VIMS group (resistant/susceptible) and laterality (left/right) was conducted for each pair of the bilateral N2 components at electrode P7/P8 and each pair of the P3 components at electrode P3/P4 (Fig. 2a and b). For the late N2 in the 260–335 ms window (N290), the RC showed a significantly enhanced amplitude compared with the CC [$F(1,24) = 32.46,\ p < 0.001$], with no group and laterality effects. For the late P3 in the 330–410 ms window (P350), amplitudes in the RC were significantly suppressed compared with those in the CC [$F(1,24) = 8.24,\ p = 0.008$], with no group and laterality effects.

As N2 is a well-known motion-onset VEP (Kubová et al., 1995; Pitzalis et al., 2012), we explore whether the individual N2 amplitude was closely associated with the vection intensity of each individual. We used linear regression models to predict the reported vection intensity of each participants by adding absolute amplitudes ($N2_{RC}$) of N223 at Pz and N290 at P7/P8, and their amplitude increments in the RC ($N2_{inc} = N2_{RC} - N2_{cc}$) as predictors. To control for other external factors, the vection response rate, vection onset delay and epoch numbers were also added in the model in a stepwise manner. Note that it is standard procedure to add all available external factors in a stepwise manner. Their inclusion in the regression analyses in no way implies that we expect them to be significant contributors. Indeed, none of the external factors had significant contribution to the model on vection intensity.

Results showed that only the increment in the N223 amplitude ($N223_{inc}$, $R^2 = 0.27$, $p = 0.006$) (see Fig. 2d for the scatter plot) and the absolute N290 amplitude at P8 ($N290_{P8\_ROT}$, $R^2 = 0.16$, $p = 0.042$) were positively associated with the average vection intensity of each participant. No significant effect was found for any model using predictors from P7. Moreover, $N223_{inc}$ was also positively associated with individual MSSQ_T ($R^2 = 0.22$) and MSSQ_C ($R^2 = 0.29$), with or without controlling for other external factors (Table 2).

3.3. Dynamic node strength in phase synchronization networks

Next, we investigated dynamic changes in node strength by comparing data collected from the RC and the CC. For the VIMS-resistant group, two significantly positive clusters were found (see Fig. 3b, d & f). The first one was located over the parietal and central regions (time window: 208–419 ms, $p = 0.005$) and the second one over the right-temporal-parietal (TP) regions (time window: 646–816 ms, $p = 0.008$). For the VIMS-susceptible group, only one positive cluster was found (see Fig. 3c and e), and it was located over the parietal midline (PM) region (time window: 281–405 ms, $p = 0.006$). No significantly negative cluster was found in either the VIMS-resistant or the susceptible group. In summary, phase synchrony was significantly enhanced when participants were exposed to coherent rotating dot patterns (CRS), supporting ***H1a***. Moreover, VIMS-resistant participants demonstrated larger (in terms of both the numbers of significant electrodes and time span) and more positive clusters than did VIMS-susceptible participants, supporting ***H1b***.

Further, we investigated the dynamic changes in node strength before

Table 2
Regression models for MSSQ scores with EEG signatures as predictors.

Predictors	MSSQ scores					
	Child scale		Adult scale		Total scale	
Single model	*Beta*	R^2	*Beta*	R^2	*Beta*	R^2
$N223_{Inc}$	0.474* (p = 0.014)	0.22 (p = 0.014)	–	–	0.474* (p = 0.014)	0.22* (p = 0.014)
$Degree_{rC\_win1}$	−0.521** (p = 0.006)	0.27** (p = 0.006)	–	–	−0.465* (p = 0.017)	0.22* (p = 0.017)
$Degree_{rTP\_win3}$	−0.518** (p = 0.007)	0.27** (p = 0.007)	−0.460* (p = 0.018)	0.21** (p = 0.018)	−0.543** (p = 0.003)	0.26** (p = 0.003)
$Degree_{rF\_win4}$	−0.559** (p = 0.003)	0.31** (p = 0.003)	−0.584** (p = 0.002)	0.34** (p = 0.002)	−0.590** (p = 0.002)	0.32** (p = 0.002)
General model		0.61*** (p < 0.001)		0.47** (p = 0.001)		0.52*** (p < 0.001)
$N223_{Inc}$	excluded		excluded		excluded	
$Degree_{rC\_win1}$	−0.383* (p = 0.015)		excluded		excluded	
$Degree_{rTP\_win3}$	−0.905** (p = 0.004)		−0.366* (p = 0.026)		−0.416** (p = 0.010)	
$Degree_{rF\_win4}$	−0.548* (p = 0.026)		−0.518** (p = 0.003)		−0.515** (p = 0.002)	

***p < 0.001; **p < 0.01; *p < 0.05. $N223_{Inc}$ = the increase in N223 amplitude in the RC after deducting the amplitude in the CC. $Degree_{rC\_win1}$ = the degree of right-central NOI (C4) in the positive subnetwork showing a higher PLV_z in the RC than in the CC in win1 (208–419 ms). $Degree_{rTP\_win3}$ = the degree of right-temporal-parietal NOI (P8) in the positive subnetwork in win3 (646–816 ms). $Degree_{rF\_win4}$ = the degree of right frontal NOIs (Fz/F4) in the negative subnetwork showing a lower PLV_z in the period after vection onset than in the period before vection onset in win4 (500–1000 ms). All significant predictors of MSSQ scores remain robust after adding the number of epochs, vection intensity and onset delay to the regression model. Note that after adding synchronization-based predictors to the stepwise model, the localization-based predictor $N223_{Inc}$ is excluded.

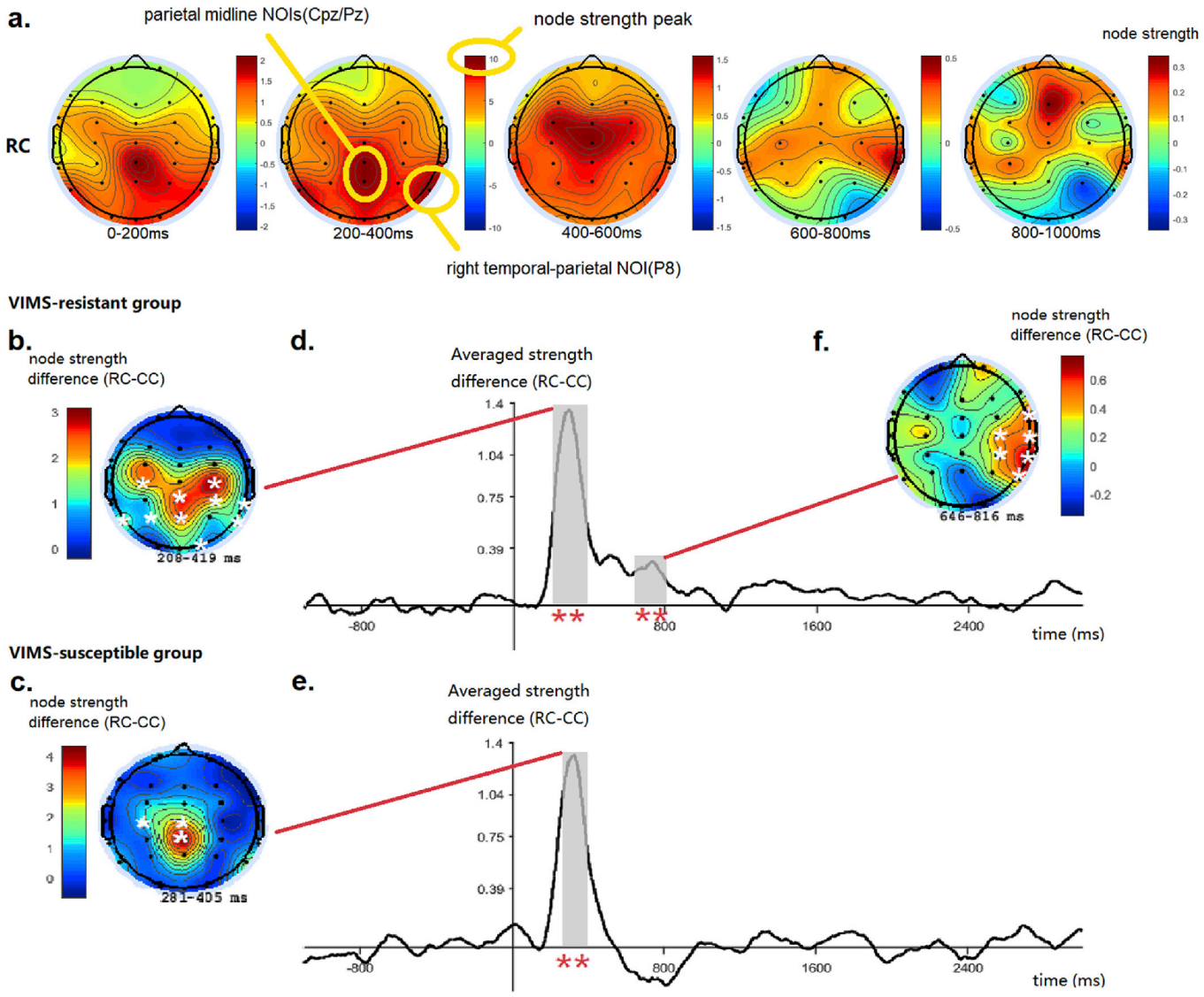

Fig. 3. Node strength in dynamic phase synchronization networks weighted by.PLV_z (a) Topography illustrating the changes in node strength in phase synchronization networks under the RC (the node strength peaks at 200–400 ms, and those nodes demonstrating the highest node strength are the dynamic hubs in the network). (b & f) Two significantly positive clusters showing a higher node strength in the RC than in the CC for the VIMS-resistant group. (c) One significantly positive cluster showing a higher node strength in the RC than in the CC for the VIMS-susceptible group. (d) The line graphs demonstrate the average node strength difference (RC subtracting CC) across all nodes for VIMS-resistant group. (e) The average node strength difference (RC subtracting CC) across all nodes for VIMS-susceptible group.

and after vection onset. For the vection condition, the event window was synchronized with the pressing of a button by the participants to indicate the onset of vection. Therefore, the period starting between 1 s before and 0.5 s after the pressing of the button was excluded from the analysis to avoid the interference from the button pressing and response delay (Kleinschmidt et al., 2002; Thilo et al., 2003). The node strength values were then averaged for a window of 500 ms to represent the node strength before and after vection onset under the same visual stimulation for each node (see Fig. 5a). Only one significant negative cluster was found in the VIMS-resistant group, which was located over the right-frontal region (see Fig. 5b, $p = 0.006$). No significant cluster was revealed in the susceptible group. In summary, the dynamic strength of phase synchronization reduced significantly after vection onset for VIMS-resistant participants, while no reduction was found for VIMS-susceptible individuals, which is consist with ***H2*** (which hypothesizes that the dynamic change in phase synchronization before and after vection onset is organized differently between the VIMS-resistant group and the VIMS-susceptible group).

3.4. Dynamic node degree in binary subnetworks connected to NOIs

As described in Section 2.4.3, centers of significant nodes in the cluster analyses (Section 3.3) were identified as NOIs. They were C4 (right-central NOI), Cpz/Pz (PM NOIs, Fig. 3b), and P8 (right TP NOI, Fig. 3f). Their node strengths were significantly higher in the RC than in the CC (note that CPz, Pz and P8 were also nodes with very high strength in the RC as shown in Fig. 3a). Fz and F4 (right-frontal NOIs) were also selected because their node strengths significantly reduced after vection onset (Fig. 5b). The corresponding cluster windows to be used for subnetwork analyses were win1 of 208–419 ms for C4; win2 of 281–405 ms for Cpz/Pz; and win3 of 646–816 ms for P8 (Appendix I). For Fz/F4, the cluster window was 500–1000 ms (win4, Appendix I3).

As the node degrees in a subnetwork for each window period can reflect the range of phase synchrony in the subnetwork, to examine whether there were intergroup differences in this range, we conducted a between-group independent-sample *t*-test for the node degrees in each subnetwork. Significantly higher node degrees were found for the

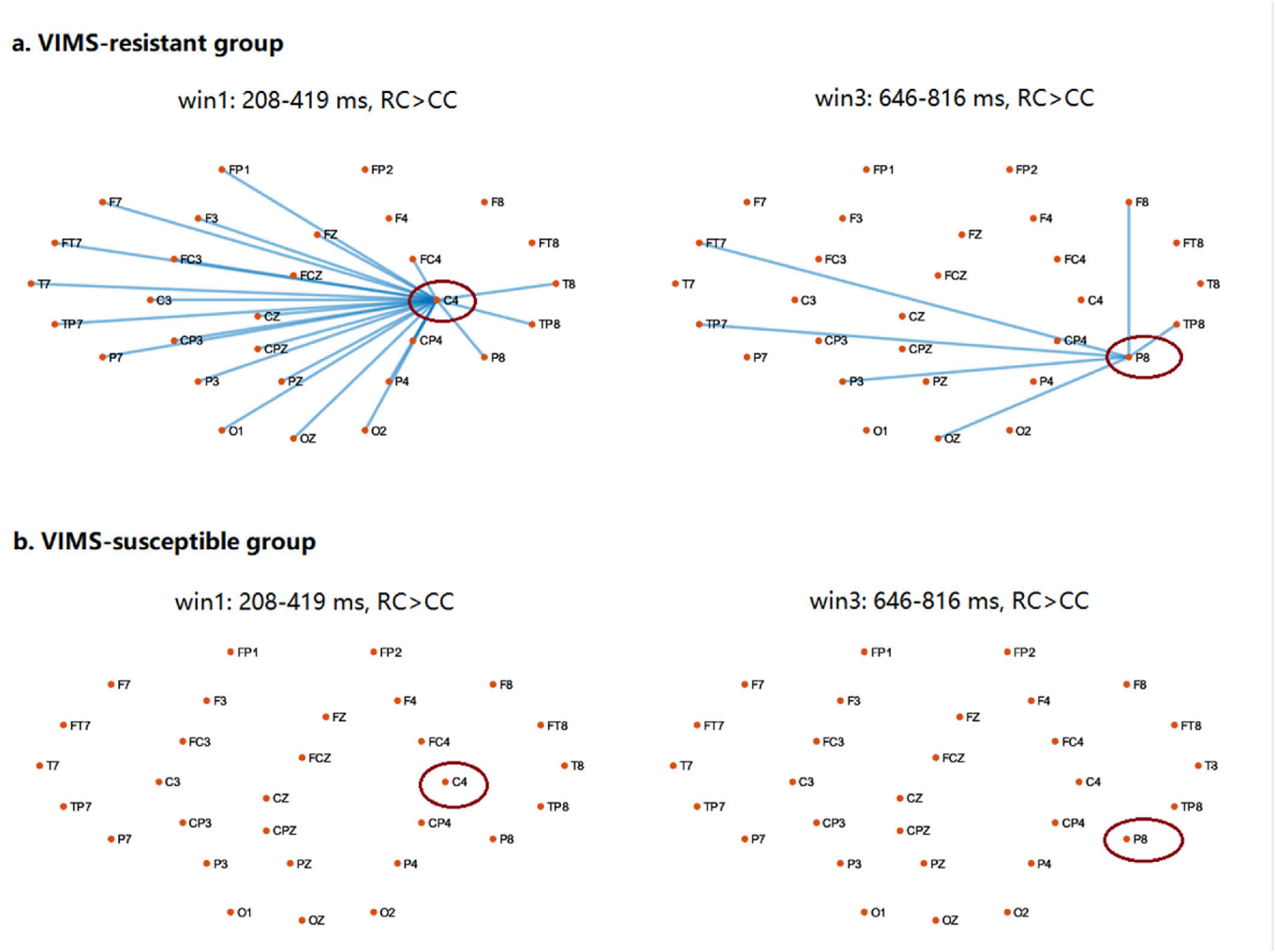

Fig. 4. Grand group subnetworks of NOIs surpassing the positive threshold (indicating a higher PLV_z in the RC than in the CC within each assessed window). (a) For the VIMS-resistant group: the left graph shows the grand group subnetwork of the right-central NOI (C4) during 208–419 ms in win1, and the right graph shows the grand group subnetwork of right-temporal-parietal NOI (P8) during 646–816 ms in win3. (b) For the VIMS-susceptible group: same as in above (a) (noted that no links surpassed the threshold in the grand group subnetwork for the VIMSsusceptible group).

VIMS-resistant group in the positive subnetworks of the right-central NOI (C4) in win1 [$t = -2.298$, $p = 0.031$], and the right TP NOI (P8) in win3 [$t = -2.800$, $p = 0.010$] (see Fig. 4 for an illustration of grand group subnetworks). Moreover, significantly higher node degrees were also found for the resistant group in the negative subnetworks of the right-frontal NOIs (Fz/F4) in win4 [$t = -3.022$, $p = 0.006$] (see Fig. 5c). No significant difference was found for Cpz/Pz in win2. In general, the VIMS-resistant group demonstrated a wider range of strengthened phase synchronization than did the VIMS-susceptible group during exposure to the coherent rotating dot pattern (CRS), supporting hypothesis ***H1b***. Moreover, after vection onset, the VIMS-resistant group showed a wider range of dynamic reductions in phase synchronization than did the VIMS-susceptible group, supporting hypothesis ***H2***.

In addition, these indexes for phase synchronization networks (node degrees in positive and negative subnetworks) were negatively correlated with the MSSQ scores (see Table 2). We constructed a stepwise regression model for each potential indicator with other control variables (vection intensity, onset delay, and epoch number) added in the model. Moreover, a general linear model was constructed for each MSSQ scale by adding all the potential predictors in a stepwise manner to find the best predictors with the highest explanatory power. Those predictors with low explanatory power and no additional contribution to the model were excluded. Table 2 presents the coefficients and explanatory power for each MSSQ scale: the upper part shows the results of models with each predictor, while the lower part shows the results of models with multiple predictors added in steps. Inspections of Table 2 indicate that combining the right-frontal NOIs (Fz/F4) (win4), right-central NOI (C4) (win1) and right TP NOI (P8) (win3) produced the highest explanatory power for the total scale among all combinations of predictors in this study [$R^2 = 0.52$, see the General model row in Table 2]. These results are robust with or without adding the vection intensity, onset delay, and epoch number in the regression model.

4. Discussion

This study identified two EEG signatures of VIMS susceptibility: excessive N2 amplitude and impaired phase synchrony dynamics. In general, dynamic cortical coordination from other cortices to the right hemisphere regions was more evident in the VIMS-resistant group than in the VIMS-susceptible group. Specifically, when exposed to VIMS-provoking stimuli, the right TP and right-central regions of VIMS-resistant individuals showed strengthened theta-band phase synchronization networks across electrodes over widely distributed brain regions (e.g. the frontal, occipital and temporal areas). Such enhancement in synchronization was limited or absent in the VIMS-susceptible group.

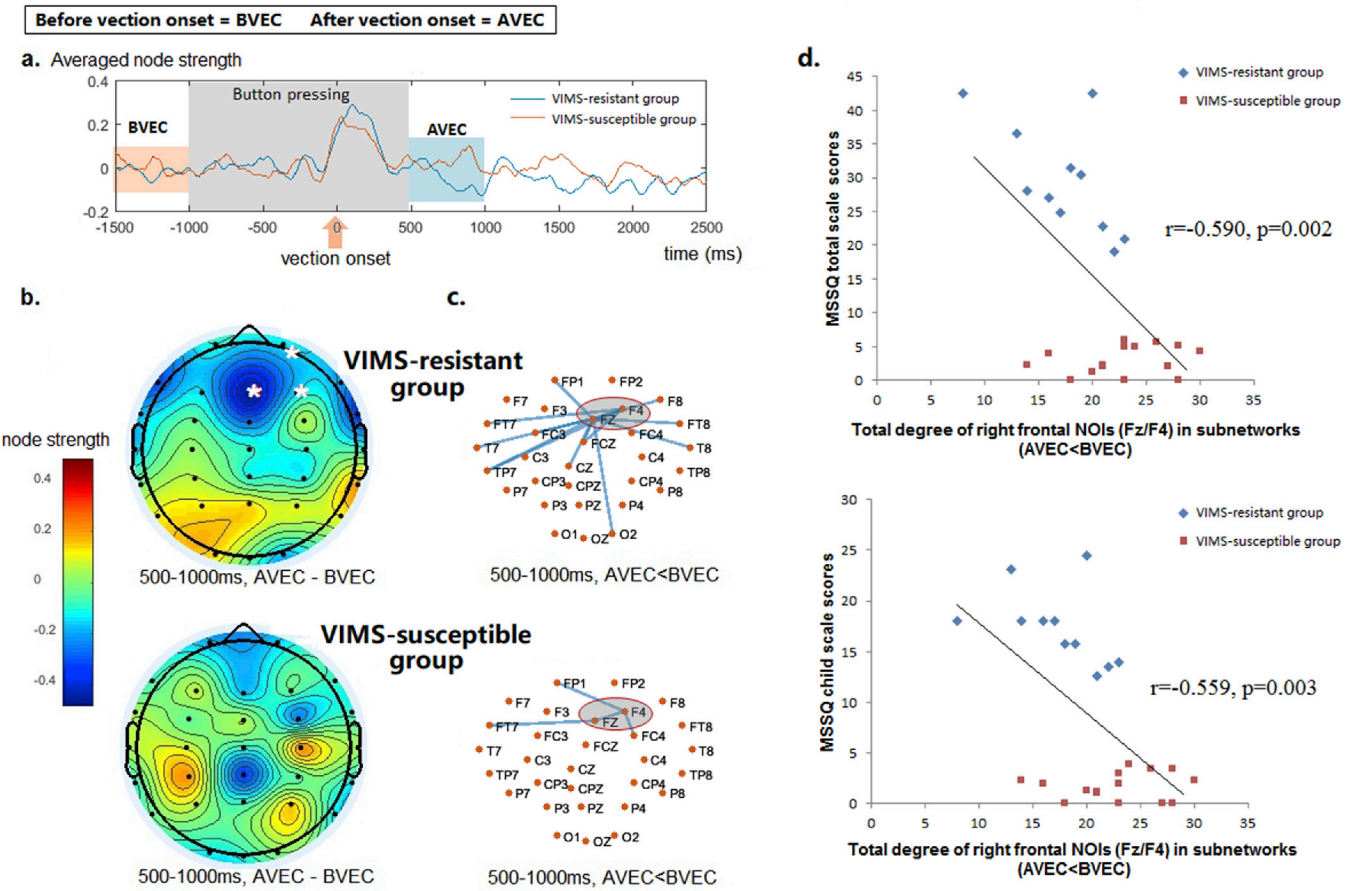

Fig. 5. Change in node strength in the phase synchronization network before and after vection onset. (a) The average node strength across all nodes for the VIMSresistant and susceptible groups with baseline corrected for the period before vection onset (−1500∼-1000 ms). (b) Significantly negative cluster in the VIMSresistant group (indicating the node strength after vecion onset [AVEC] was less than that before vection onset [BVEC]) (c) Distribution of connections to rightfrontal NOIs (Fz/F4) surpassing the negative threshold (indicating a smaller PLV_z in the period after vection onset than in the period before vection onset within the assessed window). (d) Scatter plot for of MSSQ scores of N = 26 participants and the indicator calculated from the degree of the right-frontal NOIs (Fz/F4) in the negative subnetwork (indicating a smaller PLV_z in the period after vection onset than in the period before vection onset).

Moreover, after vection onset, the strength and range of phase synchronization reduced for VIMS-resistant participants but not for VIMS-susceptible participants. This suggests that the dynamic changes in cortical coordination between sensory modalities are more active among VIMS-resistant than VIMS-susceptible individuals. The VEP results, the theta-band phase synchrony results, and their association with VIMS are discussed in detail below.

4.1. VEP components

Five VEP components with distinct spatiotemporal properties showed significantly different amplitude responses to coherent rotating dot patterns than to randomly moving dot control patterns: the attenuated P1 component (P178, in the 135–195 ms window, located in the parietal midline region), the strengthened N2 components (N223, in the 195–250 ms window, located in the PM region; N290, in the 260–335 ms window, located in the bilateral parietal regions), one of the strengthened P3 components (P305, in the 250–395 ms window, located in the PM region) and one of the attenuated P3 components (P350, in the 330–410 ms window, located in the bilateral TP region) (see Fig. 2a & b). Among the five components, only N223 showed an interaction effect between visual stimuli and VIMS susceptibility (see Fig. 2c), with excessive amplitudes reported among VIMS-susceptible participants. Moreover, increases in the amplitude of N223 ($N223_{inc}$) were also positively correlated with the MSSQ scores of participants (Table 2). This agrees with the previous finding (Chen et al., 2009) that the activity of the PM component is positively correlated with the level of VIMS. Note that although $N223_{inc}$ was also positively correlated with the vection intensity reported by participants, there were neither group differences in vection perception nor correlations between vection reports and MSSQ scores. Former findings also show that the vection magnitude is not correlated with the VIMS magnitude (Keshavarz et al., 2015b; Keshavarz and Berti, 2014). The PM region comprised rich functional areas responsible for ambient visual motion processing: the parietal-occipital visual areas (V3A and V6) (Pitzalis et al., 2013; Uesaki and Ashida, 2015; Wada et al., 2016), the precuneus motion area (PcM) (Kovács et al., 2008; Uesaki and Ashida, 2015; Wada et al., 2016), the posterior cingulate sulcus area (Field et al., 2015), and the ventral intraparietal (VIP) multisensory area (Uesaki and Ashida, 2015; Wall and Smith, 2008). Moreover, as N2 is a well-known motion-onset VEP (Kubová et al., 1995; Pitzalis et al., 2012), the enhanced amplitudes of N223 located over the PM region might reflect strong visual motion signals received by the visual modality. The absence of an excessive N223 component among VIMS-resistant participants suggests that the resistant participants might be able to suppress the large increases in the initial N2 response triggered by potentially VIMS-provoking stimulation before vection onset. As an excessive N223 is correlated with MSSQ scores, the strong visual motion signals representation in the PM region could contribute to the

development of sensory conflict and subsequently sickness symptoms if exposure to CRS continues.

The remaining four VEP components were not affected by VIMS susceptibility. They are likely associated with the visual mechanisms involved in processing the coherent rotating dot patterns that are shared by both VIMS-resistant and susceptible individuals, including ambient motion processing, spatial visual attention and vection perception. In particular, the bilateral late N2 (N290) component over the TP region (see Fig. 2) has often been reported in EEG studies using ambient visual motion stimuli (Keshavarz and Berti, 2014; Vilhelmsen et al., 2015). Moreover, in a recent study (Stróżak et al., 2016), an observable but not analyzed N2 component (observed after around 290 ms which was similar to our N2) was revealed to be stronger under larger ambient visual motion stimulation. Previous work has interpreted the amplitude of N290 (with its particular spatial-temporal properties) as reflecting general motion processing (Vilhelmsen et al., 2015) or the integration of peripheral and central motion (Keshavarz and Berti, 2014). It is worth noting that the amplitude increases of N223 and the absolute amplitudes of the right N290 positively correlated with the vection intensities reported by participants. The correlation suggests that these N2 components are related not only to the processing of ambient visual motion but also the individual perception of self-motion. Recent works have found that the N2 response varies according to the type of visual stimulus (Keshavarz and Berti, 2014; Stróżak et al., 2016; Vilhelmsen et al., 2015). Our results show for the first time that the N2 amplitude is correlated with individual vection intensity under the same visual stimulation.

The increased amplitude for the early P3 components (P305, located in the PM region) due to exposure to CRS agrees with another EEG study, which also reported increased activities in the PM region during forward visual motion stimulation spanning a large FOV (Vilhelmsen et al., 2015). P3 component observed after around 300 ms over the PM region was likely associated with increased attention arousal devoted to target and task (Herrmann and Knight, 2001). The enhanced amplitudes of P305 might reflect increasing cortical activates visual spatial attention activities during exposure to the CRS.

In addition, we found decreased VEP amplitudes in the P1/P3 time window in signals measured by the electrodes placed over the parietal-occipital regions (P178 and P350). This is consistent with past vection studies that reported a reduction in P1/P3 amplitudes at the parietal and occipital electrodes on individuals watching vection-inducing moving horizontal stripes (Keshavarz and Berti, 2014; Stróżak et al., 2016). This deactivated visual response has been interpreted as a shift from processing local visual cues to processing self-motion cues spanning a large FOV (Stróżak et al., 2016; Thilo et al., 2003). This is also consistent with past neural imaging studies, where visual areas V1/V3/V4 (Braddick et al., 2001; Kleinschmidt et al., 2002) or the Brodmann area 17/18 (Brandt et al., 1998) was found to be deactivated in individuals exposed to vection-inducing stimulation.

4.2. Theta-band phase synchronization networks

In support of hypothesis ***H1a***, theta-band phase synchronization strengthened in individuals exposed to coherent rotating dot patterns as compared with randomly moving control: the node strength of the dynamic phase synchronization network weighted by PLV_z was significantly higher in the RC than in the CC. Moreover, in support of ***H1b***, this effect was significantly stronger and covered larger cortical areas in the VIMS-resistant group than in the VIMS-susceptible group. Based on the spatiotemporal properties, these effects showed two stages.

At the earlier stage between 0.2 and 0.4 s, VIMS-resistant participants watching the coherent rotating dot patterns demonstrated increase in a large cluster of node strength, covering many nodes over the central, parietal and temporal regions (Fig. 3b), while the VIMS-susceptible participants showed increase in a smaller cluster of node strength, covering nodes restricted in the central-parietal regions (Fig. 3c). The reduced strength and size of node strength clusters among VIMS-susceptible participants may suggest that dynamic information integration with other non-visual cortical regions (especially the central region) is impaired. In the further NOI analysis, we assessed NOIs from two dominant regions: the PM region (Pz/Cpz) and the right-central region (C4). Results suggest that only the dynamic coordination with the right-central region was absent in the VIMS-susceptible group (see Fig. 4). Interestingly, this result is consistent with our previous finding using functional near-infrared spectroscopy (fNIRS). It was revealed that the hemodynamic activities from the C4 channel (from 10-20 system same as current study) could reflect the responses from somatosensory and vestibular modalities under similar visual stimulation (Zhao, 2017). Therefore, this impaired dynamic coordination with right-central regions in VIMS-susceptible individuals might indicate a lack of coordination with somatosensory and vestibular regions in the initial stage of self-motion processing.

At the later stage between 0.6 and 0.8 s, another positive cluster covering the right TP regions was found among VIMS-resistant participants, while no positive cluster was observed among VIMS-susceptible participants. Results of NOI analysis revealed that the VIMS-resistant group also had a significantly wider range of connections to the right TP NOI (P8) in the positive subnetwork. These connections were mainly distributed over the occipital and contralateral TP regions. Results suggest that the general strength and range of phase synchronization with the right TP region were impaired in VIMS-susceptible participants at this later stage. This is consistent with a recent fMRI study, where the reduced inter-hemispheric synchronization of MT + located in the TP region was reported to be associated with self-rated levels of VIMS (Miyazaki et al., 2015). White et al. (2012) showed that theta oscillations in the right TP region correlated with correct navigation performance indicating that the right TP region was associated with the integration of ego- and allo-centric representations. In this study, VEP results also reveal that the local activity of the right TP region (P8) is correlated with vection intensity. Therefore, the enhanced long-range synchronization with the right TP region found in VIMS-resistant participants might indicate the integration of self-motion information during exposure to potentially VIMS-provoking stimulation. It is possible that those dynamic links connected to the right TP region reflect the self-motion integration network that facilitates the development process related to sensory conflict reduction.

In support of hypothesis ***H2***, we found that after the onset of vection, the strength of overall cortical coordination with the frontal region (especially the right frontal region) was significantly reduced only for VIMS-resistant participants (Fig. 5b). Moreover, results of subnetwork analysis indicate that the number of reduced dynamic links after vection onset was also significantly larger for VIMS-resistant participants than for VIMS-susceptible participants (Fig. 5c). Interestingly, the number of reduced links was negatively correlated with the MSSQ scores (see the scatter plot with MSSQ_T [Beta $= -0.590$, $R^2 = 0.32$, $p = 0.002$]; and MSSQ_C [Beta $= -0.559$, $R^2 = 0.31$, $p = 0.003$] for illustration, Fig. 5d). This effect cannot be explained by the differences in exposure duration since the vection onset delay was not significantly different between the two groups (Table 1) and the number of links showing reduced phase-locking was not correlated with the length of vection delay. Previous studies also suggested that lower connectivity with the frontal region reflected less sensory mismatched information (Jo et al., 2017; Liang et al., 2017), which may explain the significant drop in cortical coordination strength between the frontal and other regions among VIMS-resistant participants observed in this study. This possibility was further supported by the fact that the magnitude of the effect described was also negatively correlated with the susceptibility of the participants.

4.3. Network signatures correlated with VIMS susceptibility

As discussed in section 4.2, we found an impaired range of theta-band

phase synchronization with the PM, right TP and right-central region among the VIMS-susceptible group exposed to coherent rotating dot patterns (Figs. 4 & 5c). The synchronization indices with the right TP region showed the strongest individual explanatory power ($R^2 = 0.34$, Table 2). Moreover, we also found that the reduced strength and range of theta-band phase-locking with the right frontal region after vection onset were negatively correlated with the MSSQ scores with a higher R^2 than other predictors including $N223_{inc}$ in the regression model (Table 2). In the general model, the combined index of the right-frontal NOIs (Fz/F4), right-central NOI (C4) and right-TP NOI (P8) produces the best explanatory power. As discussed before, it is possible that the phase-locking with the right TP region reflects the strength of sensory integration for self-motion, while the reduced communication with frontal regions (responsible for conflict detection and modulation) after vection onset indicates the individual effectiveness of conflict reduction. This agrees with the previous findings that in addition to cortical activities in the parietal-occipital regions, those in frontal regions are also associated with VIMS (Chen et al., 2009; Farmer et al., 2015; Napadow et al., 2013).

It is worth mentioning that this study focused on searching for differential EEG signatures of VIMS-susceptible and VIMS-resistant individuals before the emergence of symptoms. In this study, none of the participants experienced any obvious VIMS symptoms (including eye fatigue, disorientation and nausea), not even the VIMS-susceptible group. This confirms that our findings were not caused by VIMS symptoms. Interestingly, synchronization-based EEG signatures had much stronger explanatory power than localization-based signatures ($N223_{inc}$) on all of the MSSQ subscales. This supports our claim that sensory integration and long-range cortical interactions could contribute more to VIMS susceptibility than localized cortical activities such as regional BOLD activation. If that is the case, VIMS might be more appropriately characterized as an impairment of cortical coordination than as an abnormality in local activities.

The MSSQ used is a general questionnaire indicating motion sickness occurrence in various motion scenarios (Golding, 1998). The signatures we reported show potential properties associated with the general occurrence of sickness rather than specific stimuli used in the laboratory. Admittedly, this can also lead to the complicated situation where a participant who reports mild motion sickness in several scenarios has the same MSSQ score as a participant who reports moderate motion sickness in only one scenario. Further work differentiating the subtypes of motion sickness more meticulously is desirable.

4.4. Validations against the influence of confounding factors

To exclude the influence of possible confounding factors involved in the experimental procedures, we generated validation datasets to test the robustness of our results. First, as PLVs were calculated across all remaining clean epochs in each condition (CC/RC/VC), the number of epochs can vary among conditions. To eliminate the alternative explanation that within-subject effects might have been caused by the unequal numbers of epochs, for each participant we randomly sampled epochs in each condition to generate a smaller validation dataset to calculate PLVs. The number of epochs sampled was equal to the least remaining number of epochs. Thus, the remaining number of epochs is the same across all conditions for each participant (mean epoch number $N = 85.2 \pm 16.0$). All within-subject effects remained robust in the validation. Similarly, to exclude the influence of variations in the number of epochs at the individual level on between-subject effects, we generated another validation dataset by randomly sampling epochs in each condition, the number of which was equal to the least remaining number of epochs across all participants and all conditions. Therefore, the number of epochs ($N = 59$) used for PLV calculation was the same for all participants for all conditions. The group effects remained robust.

Another concern was that although the mean delay of vection onset was around 10 s, three participants (one from the VIMS-resistant group and two from the susceptible group) had onset delays of less than 3 s. The button pressing task for indicating vection onset might have polluted the RC epochs for these participants. To minimize the influence of button pressing, we repeated the analysis with participants who showed onset delays more than 3 s ($N = 23$). All effects remained robust. Moreover, to control for the individual variation in vection onset delay, we included onset delay in the regression models for predicting MSSQ scores and vection intensity. The explanatory power of all EEG signatures remained robust.

Finally, the current study focused on identifying EEG signatures that varied among participants with different MSSQ scores. Readers are reminded that our finding only suggests association among those variables, instead of causal relationships.

5. Conclusions

This study identified several EEG signatures of VIMS susceptibility by comparing the VEP components and phase synchronization networks between VIMS-susceptible and VIMS-resistant individuals exposed to coherent rotating dot patterns spanning a wide FOV. The experiment was meticulously designed and contributes to VIMS studies in three unique ways: 1) the EEG signatures were determined in the absence of confounding factors due to nausea symptoms; 2) to control for variations in vection perception, the EEG signatures were collected before and after vection onset under the same visual stimulation with individualized vection onset delay configured; and 3) the EEG signatures were focused on the synchronization between the local responses rather than the average local responses.

We found that a higher VIMS susceptibility is weakly associated with excessive initial local responses in parietal regions (N223) and strongly linked to impaired theta-band phase synchronization networks (especially the subnetwork with the right TP, right-frontal and right-central regions). Results are of special interest to the VIMS field. This is the first EEG study to support the sensory conflict theory from the perspective of individual differences through exploring the dynamic neural basis underlying VIMS susceptibility. Moreover, this work revealed that the variation in MSSQ scores reported by participants can be more accurately captured by the phase synchronization of cortical activities than by that of local activities, highlighting the importance of exploring global phase-locking properties. The finding has implications for the future studies on VIMS and even motion sickness in general. Our findings suggest that monitoring the global phase-locking properties can provide valuable information, which might be lost when the temporal responses are averaged under a particular type of stimulation as was done in the past.

Moreover, our method of collecting EEG signatures does not require inducing motion sickness in participants. This has the advantage that the cortical signals measured are not polluted by hyper-activities associated with motion sickness symptoms. Once validated with larger group samples in the future, these EEG signatures can be developed into applicable predictors of VIMS so that the susceptible population can take precautions and seek treatment in a timely manner. In the future, if we could combine the analyses of dynamic EEG data with imaging tools with a higher spatial resolution (e.g. MEG and fMRI), we may be able to reveal functional networks more precisely and further elucidate the neural mechanism underlying VIMS susceptibility.

Acknowledgements

The authors would like to thank the Science, Technology and Innovation Commission of Shenzhen Municipality for partially supporting the work under project no. JCYJ20170413173515472. This study was also partially funded by the Hong Kong Research Grants Council under project no. 16200915.

Appendix A. Supplementary data

Supplementary data to this article can be found online at https://doi.org/10.1016/j.neuroimage.2019.116028.

References

Aitake, M., Hori, E., Matsumoto, J., Umeno, K., Fukuda, M., Ono, T., Nishijo, H., 2011a. Sensory mismatch induces autonomic responses associated with hippocampal theta waves in rats. Behav. Brain Res. 220, 244–253. https://doi.org/10.1016/j.bbr.2011.02.011.

Aitake, M., Hori, E., Matsumoto, J., Umeno, K., Fukuda, M., Ono, T., Nishijo, H., 2011b. Sensory mismatch induces autonomic responses associated with hippocampal theta waves in rats. Behav. Brain Res. 220, 244–253. https://doi.org/10.1016/j.bbr.2011.02.011.

Araújo, D.B. de, Baffa, O., Wakai, R.T., 2002. Theta oscillations and human navigation: a magnetoencephalography study. J. Cogn. Neurosci. 14, 70–78. https://doi.org/10.1162/089892902317205339.

Berti, S., Haycock, B., Adler, J., Keshavarz, B., 2018. Early cortical processing of vection-inducing visual stimulation as measured by event-related brain potentials (ERP). Displays. https://doi.org/10.1016/j.displa.2018.10.002.

Braddick, O.J., O'Brien, J.M., Wattam-Bell, J., Atkinson, J., Hartley, T., Turner, R., 2001. Brain areas sensitive to coherent visual motion. Perception 30, 61–72.

Brainard, D.H., 1997. The psychophysics toolbox. Spat. Vis. 10, 433–436. https://doi.org/10.1163/156856897X00357.

Brandt, T., Bartenstein, P., Janek, A., Dieterich, M., 1998. Reciprocal inhibitory visual-vestibular interaction. Visual motion stimulation deactivates the parieto-insular vestibular cortex. Brain 121 (9), 1749–1758.

Brandt, T., Glasauer, S., Stephan, T., Bense, S., Yousry, T.A., Deutschlander, A., Dieterich, M., 2002. Visual-vestibular and visuovisual cortical interaction: new insights from fMRI and pet. Ann. N. Y. Acad. Sci. 956, 230–241.

Carriot, J., Brooks, J.X., Cullen, K.E., 2013. Multimodal integration of self-motion cues in the vestibular system: active versus passive translations. J. Neurosci. 33, 19555–19566. https://doi.org/10.1523/JNEUROSCI.3051-13.2013.

Chelen, W.E., Kabrisky, M., Rogers, S.K., 1993. Spectral analysis of the electroencephalographic response to motion sickness. Aviat. Space Environ. Med. 64, 24–29.

Chen, D.J., Bao, B., Zhao, Y., So, R.H.Y., 2015. Visually induced motion sickness when viewing visual oscillations of different frequencies along the fore-and-aft axis: keeping velocity versus amplitude constant. Ergonomics 0139, 1–9. https://doi.org/10.1080/00140139.2015.1078501.

Chen, D.J.Z., Chow, E.H.C., So, R.H.Y., 2011. The relationship between spatial velocity, vection, and visually induced motion sickness: an experimental study. Iperception 2, 415–415. https://doi.org/10.1068/ic415.

Chen, Y.C., Duann, J.R., Lin, C.L., Chuang, S.W., Jung, T.P., Lin, C.T., 2009. Motion-Sickness Related Brain Areas and EEG Power Activates. Springer, Berlin, Heidelberg, pp. 348–354. https://doi.org/10.1007/978-3-642-02812-0_41.

Chuang, S., Chuang, C., Yu, Y., King, J., Lin, C., 2016. EEG alpha and gamma modulators mediate motion sickness-related spectral responses. Int. J. Neural Syst. 1650007. https://doi.org/10.1142/S0129065716500076.

DeAngelis, G.C., Angelaki, D.E., 2012. Visual–Vestibular Integration for Self-Motion Perception.

Delorme, A., Makeig, S., 2004. EEGLAB: an open source toolbox for analysis of single-trial EEG dynamics including independent component analysis. J. Neurosci. Methods 134, 9–21. https://doi.org/10.1016/j.jneumeth.2003.10.009.

Dichgans, J., Brandt, T., 1978. Visual-vestibular interactions : effects of self-motion perception and postural control. Handb. Sens. Physiol. 8, 755–804.

Diels, C., Howarth, P.A., 2011. Visually induced motion sickness: single- versus dual-axis motion. Displays 32, 175–180. https://doi.org/10.1016/j.displa.2011.02.005.

Du, B., 2016. Perception of Circular Vection under Different Viewing Condtions. The Hong Kong University of Science and Technology, Clear Water Bay, Kowloon, Hong Kong. https://doi.org/10.14711/thesis-b1584878.

Farmer, A.D., Ban, V.F., Coen, S.J., Sanger, G.J., Barker, G.J., Gresty, M.A., Giampietro, V.P., Williams, S.C., Webb, D.L., Hellström, P.M., Andrews, P.L.R., Aziz, Q., 2015. Visually induced nausea causes characteristic changes in cerebral, autonomic and endocrine function in humans. J. Physiol. 593, 1183–1196. https://doi.org/10.1113/jphysiol.2014.284240.

Field, D.T., Inman, L.A., Li, L., 2015. Visual processing of optic flow and motor control in the human posterior cingulate sulcus. Cortex 71, 377–389. https://doi.org/10.1016/j.cortex.2015.07.014.

Fisher, N.I., 1993. Statistical Analysis of Circular Data. Book. Cambridge University Press, Cambridge. https://doi.org/10.1017/CBO9780511564345.

Genovese, C.R., Lazar, N.A., Nichols, T., 2002. Thresholding of statistical maps in functional neuroimaging using the false discovery rate. Neuroimage 15, 870–878. https://doi.org/10.1006/nimg.2001.1037.

Golding, J.F., 1998. Motion sickness susceptibility questionnaire revised and its relationship to other forms of sickness. Brain Res. Bull. 47, 507–516.

Graeber, D.A., Stanney, K.M., 2002. Gender differences in visually induced motion sickness. Proc. Hum. Factors Ergon. Soc. Annu. Meet. 46, 2109–2113. https://doi.org/10.1177/154193120204602602.

Griffin, M.J., 1990. Handbook of Human Vibration. Academic Press.

Guo, C.C.T., Chen, D.J.Z., Wei, I.Y., So, R.H.Y., Cheung, R.T.F., 2017. Correlations between individual susceptibility to visually induced motion sickness and decaying time constant of after-nystagmus. Appl. Ergon. 63, 1–8. https://doi.org/10.1016/j.apergo.2017.03.011.

Herrmann, C.S., Knight, R.T., 2001. Mechanisms of human attention: event-related potentials and oscillations. Neurosci. Biobehav. Rev. 25, 465–476.

Hettinger, L.J., Berbaum, K.S., Kennedy, R.S., Dunlap, W.P., Nolan, M.D., 1990. Vection and simulator sickness. Mil. Psychol. 2, 171–181. https://doi.org/10.1207/s15327876mp0203_4.

Hwang, A.D., Deng, H., Gao, Z., Peli, E., 2017. Quantifying visually induced motion sickness (VIMS) during stereoscopic 3D viewing using temporal VIMS rating. Electron. Imag. 2018, 1–9. https://doi.org/10.2352/j.imagingsci.technol.2017.61.6.060405.

ISO, 2005. Ergonomics of human-system interaction - Part 393: structured literature review of visually induced motion sickness during watching electronic imagesof human-system interaction [WWW Document]. ISO Tech. Repp. 9241–393. URL. https://www.din.de/en/getting-involved/standards-committees/naerg/projects/wdc-proj:din21:269389016. accessed 11.10.17.

Ji, J.T.T., So, R.H.Y., Cheung, R.T.F., 2009. Isolating the effects of vection and optokinetic nystagmus on optokinetic rotation-induced motion sickness. Hum. Factors 51, 739–751.

Jo, H.-G., Malinowski, P., Schmidt, S., 2017. Frontal theta dynamics during response conflict in long-term mindfulness meditators. Front. Hum. Neurosci. 11, 299. https://doi.org/10.3389/fnhum.2017.00299.

Kawasaki, M., Kitajo, K., Yamaguchi, Y., 2014. Fronto-parietal and fronto-temporal theta phase synchronization for visual and auditory-verbal working memory. Front. Psychol. 5, 200. https://doi.org/10.3389/fpsyg.2014.00200.

Kayser, J., Tenke, C.E., 2006a. Principal components analysis of Laplacian waveforms as a generic method for identifying ERP generator patterns: II. Adequacy of low-density estimates. Clin. Neurophysiol. 117, 369–380. https://doi.org/10.1016/j.clinph.2005.08.033.

Kayser, J., Tenke, C.E., 2006b. Principal components analysis of Laplacian waveforms as a generic method for identifying ERP generator patterns: I. Evaluation with auditory oddball tasks. Clin. Neurophysiol. 117, 348–368. https://doi.org/10.1016/j.clinph.2005.08.034.

Kennedy, R.S., Drexler, J., Kennedy, R.C., 2010. Research in visually induced motion sickness. Appl. Ergon. 41, 494–503. https://doi.org/10.1016/J.APERGO.2009.11.006.

Kennedy, R.S., Lane, N.E., Berbaum, K.S., Lilienthal, M.G., 1993. Simulator sickness questionnaire: an enhanced method for quantifying simulator sickness. Int. J. Aviat. Psychol. 3, 203–220. https://doi.org/10.1207/s15327108ijap0303_3.

Keshavarz, B., Berti, S., 2014. Integration of sensory information precedes the sensation of vection: a combined behavioral and event-related brain potential (ERP) study. Behav. Brain Res. 259, 131–136. https://doi.org/10.1016/j.bbr.2013.10.045.

Keshavarz, B., Campos, J.L., Berti, S., 2015a. Vection lies in the brain of the beholder: EEG parameters as an objective measurement of vection. Front. Psychol. 6. https://doi.org/10.3389/fpsyg.2015.01581.

Keshavarz, B., Hecht, H., Lawson, B., 2014. Visually Induced Motion Sickness: Causes, Characteristics, and Countermeasures, pp. 647–698. https://doi.org/10.1201/b17360-32.

Keshavarz, B., Riecke, B.E., Hettinger, L.J., Campos, J.L., 2015b. Vection and visually induced motion sickness: how are they related? Front. Psychol. 6, 472. https://doi.org/10.3389/fpsyg.2015.00472.

Kleinschmidt, A., Thilo, K.V., Büchel, C., Gresty, M.A., Bronstein, A.M., Frackowiak, R.S.J., 2002. Neural correlates of visual-motion perception as object- or self-motion. Neuroimage 16, 873–882.

Kovács, G., Raabe, M., Greenlee, M.W., 2008. Neural correlates of visually induced self-motion illusion in depth. Cerebr. Cortex 18, 1779–1787. https://doi.org/10.1093/cercor/bhm203.

Kubová, Z., Kuba, M., Spekreijse, H., Blakemore, C., 1995. Contrast dependence of motion-onset and pattern-reversal evoked potentials. Vis. Res. 35, 197–205. https://doi.org/10.1016/0042-6989(94)00138-C.

Lachaux, Jean-Philippe Rodriguez, E., Le van Quyen, M., Lutz, A., Martinerie, J., Varela, F.J., 2000. Studying single-trials of phase synchronous activity in the brain. Int. J. Bifurc. Chaos 10, 2429–2439. https://doi.org/10.1142/S0218127400001560.

Lachaux, J.P., Rodriguez, E., Martinerie, J., Varela, F.J., 1999. Measuring phase synchrony in brain signals. Hum. Brain Mapp. 8, 194–208.

Le, A.T.D., Payne, J., Clarke, C., Kelly, M.A., Prudenziati, F., Armsby, E., Penacchio, O., Wilkins, A.J., 2017. Discomfort from urban scenes: metabolic consequences. Landsc. Urban Plan. 160, 61–68. https://doi.org/10.1016/j.landurbplan.2016.12.003.

Liang, T., Hu, Z., Liu, Q., 2017. Frontal theta activity supports detecting mismatched information in visual working memory. Front. Psychol. 8, 1821. https://doi.org/10.3389/FPSYG.2017.01821.

Maris, E., Oostenveld, R., 2007. Nonparametric statistical testing of EEG- and MEG-data. J. Neurosci. Methods 164, 177–190. https://doi.org/10.1016/j.jneumeth.2007.03.024.

Miyazaki, J., Yamamoto, H., Ichimura, Y., Yamashiro, H., Murase, T., Yamamoto, T., Umeda, M., Higuchi, T., 2015. Inter-hemispheric desynchronization of the human MT + during visually induced motion sickness. Exp. Brain Res. https://doi.org/10.1007/s00221-015-4312-y.

Mognon, A., Jovicich, J., Bruzzone, L., Buiatti, M., 2011. ADJUST: an automatic EEG artifact detector based on the joint use of spatial and temporal features. Psychophysiology 48, 229–240. https://doi.org/10.1111/j.1469-8986.2010.01061.x.

Murray, M., Wallace, M., 2011. The Neural Bases of Multisensory Processes. https://doi.org/10.1201/b11092.

Napadow, V., Sheehan, J.D., Kim, J., Lacount, L.T., Park, K., Kaptchuk, T.J., Rosen, B.R., Kuo, B., 2013. The brain circuitry underlying the temporal evolution of nausea in humans. Cereb. Cortex 23, 806–813. https://doi.org/10.1093/cercor/bhs073.

Nesbitt, K., Davis, S., Blackmore, K., Nalivaiko, E., 2017. Correlating reaction time and nausea measures with traditional measures of cybersickness. Displays 48, 1–8. https://doi.org/10.1016/j.displa.2017.01.002.

Nooij, S.A.E., Pretto, P., Oberfeld, D., Hecht, H., Bülthoff, H.H., 2017. Vection is the main contributor to motion sickness induced by visual yaw rotation: implications for conflict and eye movement theories. PLoS One 12. https://doi.org/10.1371/journal.pone.0175305.

Oman, C.M., Cullen, K.E., 2014. Brainstem processing of vestibular sensory exafference: implications for motion sickness etiology. Exp. Brain Res. 232, 2483–2492. https://doi.org/10.1007/s00221-014-3973-2.

Oostenveld, R., Fries, P., Maris, E., Schoffelen, J.M., 2011. FieldTrip: open source software for advanced analysis of MEG, EEG, and invasive electrophysiological data. Comput. Intell. Neurosci. 2011, 156869. https://doi.org/10.1155/2011/156869.

Palmisano, S., Arcioni, B., Stapley, P.J., 2018. Predicting vection and visually induced motion sickness based on spontaneous postural activity. Exp. Brain Res. 236, 315–329. https://doi.org/10.1007/s00221-017-5130-1.

Pelli, D.G., 1997. The VideoToolbox software for visual psychophysics: transforming numbers into movies. Spat. Vis. 10, 437–442. https://doi.org/10.1163/156856897X00366.

Pitzalis, S., Bozzacchi, C., Bultrini, A., Fattori, P., Galletti, C., Di Russo, F., 2013. Parallel motion signals to the medial and lateral motion areas V6 and MT+. Neuroimage 67, 89–100. https://doi.org/10.1016/j.neuroimage.2012.11.022.

Pitzalis, S., Strappini, F., De Gasperis, M., Bultrini, A., Di Russo, F., 2012. Spatio-temporal brain mapping of motion-onset VEPs combined with fMRI and retinotopic maps. PLoS One 7, e35771. https://doi.org/10.1371/journal.pone.0035771.

Reason, J.T., 1978. Motion sickness adaptation: a neural mismatch model. J. R. Soc. Med. 71, 819–829.

Rebenitsch, L., Owen, C., 2016. Review on cybersickness in applications and visual displays. Virtual Real. 20, 101–125. https://doi.org/10.1007/s10055-016-0285-9.

Sheehan, J., LaCount, L., Kim, J., Lee, J., John, S., Newman, S., Foy, C., Michalek, W., Park, K., Kuo, B., Napadow, V., Lic, A., 2009. Neural correlates of motion sickness induced nausea - an fMRI study. Neuroimage 47, S84. https://doi.org/10.1016/S1053-8119(09)70620-2.

So, R.H.Y., Ujike, H., 2010. Visually induced motion sickness, visual stress and photosensitive epileptic seizures: what do they have in common? - preface to the special issue. Appl. Ergon.

Stanney, K.M., Kingdon, K.S., Kennedy, R.S., 2002. Dropouts and aftereffects: examining general accessibility to virtual environment Technology. Proc. Hum. Factors Ergon. Soc. Annu. Meet. 46, 2114–2118. https://doi.org/10.1177/154193120204602603.

Stróżak, P., Francuz, P., Augustynowicz, P., Ratomska, M., Fudali-Czyż, A., Bałaj, B., 2016. ERPs in an oddball task under vection-inducing visual stimulation. Exp. Brain Res. 1–10. https://doi.org/10.1007/s00221-016-4748-8.

Sun, J., Hong, X., Tong, S., 2012. Phase synchronization analysis of eeg signals: an evaluation based on surrogate tests. IEEE Trans. Biomed. Eng. 59, 2254–2263. https://doi.org/10.1109/TBME.2012.2199490.

Thilo, K.V., Kleinschmidt, A., Gresty, M.A., 2003. Perception of self-motion from peripheral optokinetic stimulation suppresses visual evoked responses to central stimuli. J. Neurophysiol. 90, 723–730. https://doi.org/10.1152/jn.00880.2002.

Totah, N.K.B., Jackson, M.E., Moghaddam, B., 2013. Preparatory attention relies on dynamic interactions between prelimbic cortex and anterior cingulate cortex. Cerebr. Cortex 23, 729–738. https://doi.org/10.1093/cercor/bhs057.

Uesaki, M., Ashida, H., 2015. Optic-flow selective cortical sensory regions associated with self-reported states of vection. Front. Psychol. 6, 775. https://doi.org/10.3389/fpsyg.2015.00775.

Varela, F., Lachaux, J.P., Rodriguez, E., Martinerie, J., 2001. The brainweb: phase synchronization and large-scale integration. Nat. Rev. Neurosci. 2, 229–239. https://doi.org/10.1038/35067550.

Vilhelmsen, K., van der Weel, F.R., Ruud), van der Meer, A.L.H., 2015. A high-density EEG study of differences between three high speeds of simulated forward motion from optic flow in adult participants. Front. Syst. Neurosci. 9. https://doi.org/10.3389/fnsys.2015.00146.

Wada, A., Sakano, Y., Ando, H., 2016. Differential responses to a visual self-motion signal in human medial cortical regions revealed by wide-view stimulation. Front. Psychol. 7, 309. https://doi.org/10.3389/fpsyg.2016.00309.

Wall, M.B., Smith, A.T., 2008. The representation of egomotion in the human brain. Curr. Biol. 18, 191–194. https://doi.org/10.1016/j.cub.2007.12.053.

Webb, N.A., Griffin, M.J., 2003. Eye movement, vection, and motion sickness with foveal and peripheral vision. Aviat. Space Environ. Med. 74, 622–625.

Wei, Y., Zheng, J., So, R.H.Y., 2018. Allocating less attention to central vision during vection is correlated with less motion sickness. Ergonomics 1–14. https://doi.org/10.1080/00140139.2018.1427805.

White, D.J., Congedo, M., Ciorciari, J., Silberstein, R.B., 2012. Brain oscillatory activity during spatial navigation: theta and gamma activity link medial temporal and parietal regions. J. Cogn. Neurosci. 24, 686–697. https://doi.org/10.1162/jocn_a_00098.

Wilkins, A., 2016. A physiological basis for visual discomfort: application in lighting design. Light. Res. Technol. 48, 44–54. https://doi.org/10.1177/1477153515612526.

Winkler, A.M., Webster, M.A., Brooks, J.C., Tracey, I., Smith, S.M., Nichols, T.E., 2016. Non-parametric combination and related permutation tests for neuroimaging. Hum. Brain Mapp. 37, 1486–1511. https://doi.org/10.1002/hbm.23115.

Yokota, Y., Aoki, M., Mizuta, K., Ito, Y., Isu, N., 2005. Motion sickness susceptibility associated with visually induced postural instability and cardiac autonomic responses in healthy subjects. Acta Otolaryngol. 125, 280–285. https://doi.org/10.1080/00016480510003192.

Zhang, L.-L., Wang, J.-Q., Qi, R.-R., Pan, L.-L., Li, M., Cai, Y.-L., 2015. Motion sickness: current knowledge and recent advance. CNS Neurosci. Ther. https://doi.org/10.1111/cns.12468. n/a-n/a.

Zhao, Y., 2017. Identifying Vestibular and Visual Cortical Response during Circular Vection Among People with Different Susceptibility to Motion Sickness. The Hong Kong University of Science and Technology, Clear Water Bay, Kowloon, Hong Kong. https://doi.org/10.14711/thesis-b1781036.